International Journal of Heat and Mass Transfer 122 (2018) 707–718

Contents lists available at ScienceDirect

International Journal of Heat and Mass Transfer

journal homepage: www.elsevier.com/locate/ijhmt

An experimental investigation on the unsteady heat transfer process over an ice accreting airfoil surface

Yang Liu, Hui Hu *

Department of Aerospace Engineering, Iowa State University, 1200 Howe Hal, 537 Bissell Road, Ames, IA 50011-1096, USA

ARTICLE INFO

Article history:
Received 21 December 2017
Accepted 6 February 2018
Available online 20 February 2018

Keywords:
Unsteady heat transfer
Dynamic ice accretion
Multiphase flow
Convective heat transfer
Infrared thermal imaging

ABSTRACT

In the present study, an experimental investigation was performed in an Icing Research Tunnel available at Iowa State University (i.e., ISU-IRT) to quantify the unsteady heat transfer and dynamic ice accretion process over an airfoil/wing surface under different icing conditions (i.e., dry rime ice accretion vs. wet glaze ice accretion). A theoretic model was developed at first to evaluate the unsteady heat transfer process over the ice accreting airfoil/wing surface in the term of convective heat transfer coefficient. During the experiments, a high-speed infrared (IR) thermal imaging system was used to achieve temporally-resolved measurements of the surface temperature distribution over the ice accreting airfoil/wing surface. The transient behaviors of droplets impingement, surface water runback and dynamic phase changing processes over the airfoil/wing surface were characterized quantitatively based on the quantitative surface temperature measurements. Based on the time evolution of the measured surface temperature distributions over the airfoil/wing surface for the rime ice accretion case, the water collection efficiency distribution around the airfoil surface was determined quantitatively, which was then imported into the theoretic heat transfer model to estimate the convective heat transfer coefficients over the ice accreting airfoil/wing surface. The convective heat transfer coefficient was found to reach its maximum value at the airfoil stagnation point, and decrease gradually at the downstream locations. The formation of the ice roughness near the airfoil leading edge was found to be able to enhance the convective heat transfer process over the airfoil surface, which would further promote the ice formation and accretion over the roughed airfoil surface.

1. Introduction

Aircraft icing is widely recognized as a significant aviation hazard to aircraft operation in cold weather. While the most familiar and frequently observed aircraft icing events are the ice buildup over airframe surfaces with airplanes being exposed to frozen precipitation at airports, such icing hazard can be easily overcome by applying de-/anti-icing fluids over the airframe surfaces prior to takeoff [1]. In-flight aircraft icing occurs when small, super-cooled, airborne water droplets, which make up clouds and fog, freeze upon impacting onto airframe surfaces. Since the airborne water droplets are in a super-cooled state, they can either freeze immediately or become mixtures of liquid water and ice upon impinging onto airframe surfaces, depending on the ambient conditions [2]. Ice accretion over in-flight aircraft surfaces was found not only to result in a significant decrease in lift and a rapid rise in drag, but also to induce unstable control conditions when ice accumulates asymmetrically on aircraft control surfaces [3]. The importance of proper in-flight aircraft icing control was highlighted by many aircraft crashes in recent years like the deadly accident occurred at Clarence Center, New York on 02/12/2009 with fifty fatalities in the accident of a Bombardier DHC-8-400 aircraft operated as Continental Flight 3407 [4].

It is well known that ice accretion process over the surface of an in-flight airplane can be either wet (glaze) or dry (rime), depending on ambient conditions [5]. When an airplane encounters clouds with low liquid water content (LWC) and small-sized super-cooled water droplets at relatively low ambient temperature (i.e., typically below −8 °C), rime ice would usually form as the super-cooled water droplets freeze immediately upon impact. In rime icing conditions, the released latent heat of fusion due to phase change of the impinged super-cooled water droplets would be removed efficiently through heat transfer, and no surface water flow would exist over the airframe surfaces [2]. The amount and rate of ice accretion over the airframe surfaces would be solely determined by the impingement behavior of the super-cooled water droplets [2]. Glaze icing process was found to be associated

* Corresponding author.
E-mail address: huhui@iastate.edu (H. Hu).

https://doi.org/10.1016/j.ijheatmasstransfer.2018.02.023
0017-9310/

with warmer ambient temperatures (i.e., usually above −8 °C), higher liquid water contents in clouds, and larger super-cooled water droplets. In glaze icing conditions, while the heat transfer is insufficient to remove all the released latent heat of fusion of the impinged super-cooled water droplets, only a portion of the impinged super-cooled water droplets would freeze upon impact, and the remaining would remain in liquid as unfrozen water and run back over the airframe surfaces, as driven by the boundary layer airflow over the aircraft surface [2,6,7]. As a result, the amount and rate of glaze ice accretion over the airframe surfaces are mainly determined by the heat transfer capacity to remove the latent heat of fusion of the impinged supper-cooled water droplets over the ice accreting surface [3,8–10].

A number of engineering software tools (e.g., TURBICE and LEWICE) have been developed in recent years to predict the ice accretion process for various aircraft icing mitigation applications [11–15]. Such packages utilize airflow speed, temperature, accretion time, liquid water content and droplet size as input data to predict the shape and amount of resulting ice accretion on airfoil/wing surfaces. It was found that, due to the very complex interactions among multiphase flows (i.e., the boundary layer airflow, super-cooled water droplets and surface water runback flows, and ice accreting process over airframe surface) and the unsteady mass and heat transfer processes associated with the dynamic impingement of the super-cooled water droplets, transient surface water transport and the dynamic solidification (i.e., phase changing) process, the accurate prediction of ice accretion over airframe surfaces, especially for the glaze ice accretion case, was still very challenging [16]. While the ice accretion tools usually include classical models and correlations for various multiphase components which are assumed to contribute to the ice formation and accretion processes, many important details of the complex coupled multiphase micro-physical processes associated with the dynamic ice accretion process were usually ignored [6,17,18]. Such simplistic evaluation of the transient behavior of surface water transport and unsteady heat transfer process is considered to be a significant contributing factor in the poor agreement between the predictions of the theoretical models and the experimental results about glaze ice accretion process [14,19–21].

Advancing the technology for safe and efficient operation of aircraft in atmospheric icing conditions requires the development of innovative, effective anti-/de-icing strategies for aircraft icing mitigation and protection. Doing so requires a keen understanding of the underlying physics of complicated thermal flow processes pertinent to aircraft icing phenomena, both for the icing itself as well as for the unsteady heat transfer and dynamic water runback along ice accreting airframe surfaces. While a number of previous studies have been carried out to simulate ice formation and accretion on airfoil/wing models through icing wind tunnel testing [8,22,23] or using "artificial" iced profiles with various types and amounts of ice accretion to investigate the aerodynamic performance degradation for iced airfoils/wings [24–26], very few fundamental studies can be found in literature to elucidate the underlying physics of the dynamic ice accreting process. Many important micro-physical processes associated with aircraft icing phenomena, such as characteristics of the unsteady heat transfer and dynamic phase changing processes over ice accreting airfoil/wing surfaces, are still not fully explored.

In the present study, we reported an experimental investigation to quantify the unsteady heat transfer and dynamic phase changing processes as super-cooled water droplets impacting onto the surface of an airfoil/wing model under different icing conditions (i.e., both dry rime and wet glaze icing conditions) to elucidate the underlying icing physics pertinent to aircraft icing phenomena. In the context that follows, a theoretic model was developed at first to evaluate the unsteady convective heat transfer process over an ice accreting airfoil/wing surface. By leveraging the unique Icing Research Tunnel available at Iowa State University (i.e., ISU-IRT), a comprehensive experimental campaign was conducted to investigate the unsteady heat transfer and dynamic phase changing processes over an ice accreting airfoil/wing surfaces under both rime and glaze conditions. During the experiments, an infrared (IR) thermal imaging system was used to achieve spatially-and-temporally-resolved temperature distribution measurements over the airfoil/wing surface during the dynamic ice accretion process. The characteristics of the unsteady heat transfer and transient behaviors of the surface water runback process over the ice accreting airfoil/wing surface were examined quantitatively in the course of the dynamic ice accretion process. Based on the spatially-and-tempo rally-resolved temperature measurements around the leading edge of the airfoil/wing model, the distribution of water collection efficiency around the airfoil leading edge was derived quantitatively, which was then imported into the convective heat transfer model to further evaluate the unsteady heat transfer characteristics over the ice accreting airfoil/wing surface.

2. Theoretical analysis of unsteady heat transfer over an ice accreting airfoil surface

In the present study, the energy conservation law was applied to an arbitrarily-chosen control volume over an ice accreting airfoil/wing surface in order to evaluate the unsteady heat transfer process over the airfoil/wing surface. As shown schematically in Fig. 1, the rate at which the thermal and/or mechanical energies enter into the control volume, minus the rate at which the thermal and mechanical energies leave from the control volume would be balanced by the rate of net energy increase stored within the control volume [27], which can be expressed as:

$$\dot{E}_{in} - \dot{E}_{out} = \frac{dE_{st}}{dt} \equiv \dot{E}_{st} \tag{1}$$

where $\dot{E}_{in}$ is the rate of energy enters the control volume, $\dot{E}_{out}$ is the rate of energy leaves the control volume, and $\dot{E}_{st}$ is rate of the net energy increase stored inside the control volume.

The energy enters the control volume includes adiabatic heating and kinetic heating energy. The energy leaves the control volume includes the evaporation and sublimation, convection heat, energy radiation, conduction heat, and sensible heat that is produced by the temperature changes of the water and ice over the surfaces of the control volume [6,18]. The net energy increase stored inside the control volume are due to the changes in the internal, kinetic, and/or potential energies of its contents [27], which is given as following:

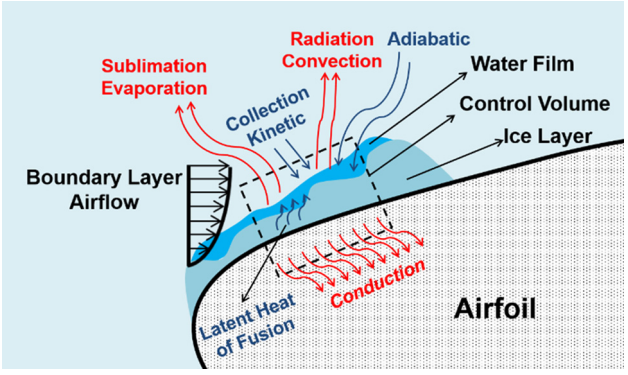

Fig. 1. A schematic of energy balance in an arbitrarily-chosen control volume over an ice accreting airfoil/wing surface.

$$\Delta E_{st} = \Delta U + \Delta KE + \Delta PE \tag{2}$$

where ΔU is the change in internal energy, ΔKE is the change of kinetic energy, ΔPE is the change in potential energy inside the control volume.

During the ice accretion process over an airfoil/wing surface, the changes of kinetic and potential energy inside the control volume are usually several orders of magnitude smaller in comparison to the change in internal energy, thereby, can be neglected. When super-cooled water droplets impinge onto the airfoil/wing surfaces, there will be a phase transition of the super-cooled water droplets from liquid into solid state to give off energy (i.e., known as the latent heat of fusion) due to the changes in the intermolecular forces, and less from a sensible component that accounts for the motion of the atoms/molecules. Thus, the net energy increase stored inside the control volume is reduced, which can be expressed as:

$$\dot{E}_{st} = -(\dot{Q}_{latent} + \dot{Q}_{ss}) \tag{3}$$

where Q_{latent} is the latent heat of fusion, Q_{ss} is the sensible heat.

Therefore, the energy conservation law in the control volume can be expressed as:

$$[\dot{Q}_{adh} + \dot{Q}_{kin}] - [\dot{Q}_{conv} + \dot{Q}_{sub/evp} + \dot{Q}_{cond}] = -(\dot{Q}_{latent} + \dot{Q}_{ss}) \tag{4}$$

where Q_{adh} is the adiabatic heating, Q_{kin} is the kinetic heating, Q_{conv} is the convective heat, Q_{sub} is the sublimation heat, Q_{evp} is the evaporation heat, Q_{cond} is the conductive heat.

The heat introduced by adiabatic heating occurring inside of the boundary layer is defined as:

$$\dot{Q}_{adh} = h_{cv} \cdot (T_{rec} - T_{air,\infty}) \cdot A \tag{5}$$

where h_{cv} is the convective heat transfer coefficient, T_{rec} is the recovery temperature, $T_{air,\infty}$ is the free stream temperature, and A is the panel surface area.

The recovery temperature, T_{rec} in Eq. (5) is originally defined by Schlichting [28]. It has been implemented in the modelling of heat transfer for ice formation, as can be found in Fortin [6].

$$T_{rec} = T_{\infty} + r \cdot \frac{T_{\infty}}{T_e} \cdot \frac{U_e^2}{2 \cdot C_{air}} \tag{6}$$

where T_e is the temperature at the edge of the boundary layer, U_e is the speed at the edge of the boundary layer, C_{air} is the specific heat of air, r is the recovery factor that can be defined as $r = \sqrt{Pr}$. Here, the Prandtl number is defined as:

$$Pr = \frac{C_{air} \cdot \mu_{air}}{k_{air}} \tag{7}$$

where μ_{air} is the dynamic viscosity of air, and k_{air} is the thermal conductivity of air.

The impingement of the super-cooled water droplets would introduce kinetic energy into the control volume, which can be expressed:

$$\dot{Q}_{kin} = \frac{1}{2} \cdot \dot{m}_{imp} \cdot V_{imp}^2 \tag{8}$$

where $\dot{m}_{imp}$ is the mass flux of water impingement, and can be defined as $\dot{m}_{imp} = LWC \times V_{imp} \times A$ in the region very near the stagnation line; where V_{imp} is the impact speed of the super-cooled water droplets, LWC is the liquid water content in the incoming airflow.

The convective heat transfer would occur when cold air flows over the airfoil surface. As describe in Incropera [27], the convection term in the energy equation can be expressed as:

$$\dot{Q}_{conv} = h_{cv} \cdot (T_{surf} - T_{air,\infty}) \cdot A \tag{9}$$

where T_{surf} is the surface temperature.

The heat in the control volume can also be transferred to the surroundings by evaporation and sublimation. As described in Li [29] and Dong [30], the mass flux due to evaporation and sublimation can be usually estimated using:

$$\dot{m}_{es} = 0.696 \cdot \frac{h_{cv}}{C_{air}} \cdot \frac{p_s(T_b) - p_s(T_{\infty})}{p_m} \cdot A \tag{10}$$

where the saturated vapor pressures, $p_s(T_b)$ and $p_s(T_{\infty})$ are obtained by using Goff-Gratch equation [31]. T_b is the water film temperature, and P_m is the average of wall pressure and free stream pressure. Thus, the latent heat of evaporation and sublimation can be calculated by using following equation:

$$\dot{Q}_{sub/evp} = \dot{m}_{es} \cdot [\eta \cdot L_i + (1 - \eta) \cdot L_w] \tag{11}$$

where m_{es} is the mass of evaporation and sublimation, L_i is the latent heat of sublimation of ice, L_w is the latent heat of vaporization of water, η is the local freezing fraction.

Conductive heat transfer would occur if there is a temperature gradient between the ice/water and the substrate of the airfoil/wing model. The heat flux due to thermal conduction is given as:

$$\dot{Q}_{cond} = \frac{A \cdot (T_{surf} - T_{airfoil})}{R_{tot,cond}} \tag{12}$$

where $T_{airfoil}$ is the surface temperature of the airfoil substrate, $R_{tot,cond}$ is the equivalent thermal resistance for conduction, which can be derived based on the *equivalent thermal circuit* theory:

$$R_{tot,cond} = \frac{H_{ice}}{k_{ice}} + \frac{H_{airfoil}}{k_{airfoil}} \tag{13}$$

where H_{ice} is the thickness of ice layer, $H_{airfoil}$ is the thickness of airfoil substrate, k_{ice} is the thermal conductivity of ice, and $k_{airfoil}$ is the thermal conductivity of airfoil substrate. At the initial stage of ice accretion, the ice thickness is very small (i.e., usually two orders smaller than the thickness of airfoil substrate), while the thermal conductivity of ice is much greater than that of the plastic airfoil model used in the present study, Eq. (13) can be reduced to $R_{tot,cond} = H_{airfoil}/k_{airfoil}$. Therefore, the heat flux due to thermal conduction can be derived as:

$$\dot{Q}_{cond} = \frac{k_{airfoil} \cdot A \cdot (T_{surf} - T_{airfoil})}{H_{airfoil}} \tag{14}$$

The latent heat of fusion would be released when water freezes over the airfoil surface. The amount of the latent heat released in the control volume is dependent on the mass of the frozen water, which can be written as:

$$Q_{latent} = m_{freeze} \cdot L_s \tag{15}$$

where m_{freeze} is the mass of the frozen water, L_s is the latent heat released per unit water mass.

Within the control volume, the liquid water mass is mainly from the impinging water mass and the incoming runback water mass. The amount of ice accumulated inside the control volume is determined by the freezing fraction, η, which is defined as the mass ratio of the frozen water to the total of water collection in the control volume. Thus, the freezing rate in the control volume can be expressed as:

$$\dot{m}_{freeze} = [\dot{m}_{runin} \cdot A + LWC \cdot V_{imp} \cdot A \cdot \beta] \cdot \eta \tag{16}$$

where m_{runin} is the incoming runback water mass per unit of area, and β is the local water collection efficiency.

Then, the heat flux due to the latent heat of fusion can be derived as:

$$\dot{Q}_{latent} = \dot{m}_{freeze} \cdot L_s = [\dot{m}_{runin} + LWC \cdot V_{imp} \cdot \beta] \cdot A \cdot \eta \cdot L_s \tag{17}$$

The sensible heat is mainly due to the enthalpy variation of frozen and liquid water from the freezing temperature to the surface temperature, which can be expressed as:

$$\dot{Q}_{ss} = \dot{m}_{freeze} \cdot C_i \cdot (T_f - T_{surf}) + (\dot{m}_w - \dot{m}_{freeze}) \cdot C_w \cdot (T_f - T_{surf}) \quad (18)$$

where C_i is the specific heat of ice, C_w is the specific heat of water. Here, $\dot{m}_w$ is the mass flux of water in the control volume. Within the control volume, $\dot{m}_w \approx \dot{m}_{runin} \cdot A + LWC \cdot V_{imp} \cdot A \cdot \beta$. By substituting Eqs. (5), (8), (9), (11), (14), (17) and (18) into Eq. (4), the energy conservation equation can be expressed as following:

$$\begin{aligned} &h_{cv} \cdot (T_{rec} - T_{air,\infty}) \cdot A + \frac{1}{2} \cdot LWC \cdot V_{imp} \cdot A \cdot V_{imp}^2 + [\dot{m}_{runin} \cdot A \\ &\quad + LWC \cdot V_{imp} \cdot A \cdot \beta] \cdot [\eta \cdot L_s + (T_f - T_{surf}) \cdot (\eta \cdot C_i + (1-\eta) \cdot C_w)] \\ &= A \cdot [h_{cv} \cdot (T_{surf} - T_{air,\infty})] + A \cdot (T_{surf} - T_{airfoil}) / R_{cond,tot} \\ &\quad + 0.696 \cdot h_{cv} / C_a \cdot [p_s(T_b) - p_s(T_\infty)] / p_m \cdot A \cdot [\eta \cdot L_i + (1-\eta) \cdot L_w] \end{aligned} \quad (19)$$

In the present study, since the temperature of the airfoil/wing model and the incoming airflow temperature were at the same values during the experiments, the terms of temperature differences in the heat convection and heat conduction can be considered as the same, and denoted as ΔT. Therefore, the convection heat transfer coefficient, h_{cv} over the ice accreting airfoil/wing surface can be derived as following:

$$h_{cv} = \frac{[\Delta T / R_{cond,tot} - (\dot{m}_{runin} + LWC \cdot V_{imp} \cdot \beta)[\eta \cdot L_s + (T_f - T_{surf}) \cdot (\eta \cdot C_i + (1-\eta) \cdot C_w)] - 0.5 \cdot LWC \cdot V_{imp}^3]}{[T_{rec} - T_{air,\infty} - \Delta T - 0.696 \cdot [p_s(T_b) - p_s(T_{air,\infty})] / (C_a \cdot p_m) \cdot [\eta \cdot L_i + (1-\eta) \cdot L_w]]} \quad (20)$$

In the present study, by leveraging the unique Icing Research Tunnel available at Iowa State University (ISU-IRT), a comprehensive experimental campaign was performed to examine the transient behavior of the convective heat transfer over an ice accreting airfoil/wing surface under different icing conditions. With the quantitative measurements of the surface temperature distributions over the ice accreting airfoil/wing surfaces obtained through the experiment campaign, along with the relevant controlling parameters such as the water collection efficiency (β), the time evolution of the convective heat transfer coefficient over the ice accreting airfoil/wing surfaces in the course of dynamic ice accretion process will be evaluated quantitatively by using Eq. (20).

3. Experimental setup and test model

The experimental study was performed in a newly-refurbished Icing Research Tunnel available at Iowa State University (ISU-IRT). As shown schematically in Fig. 2, ISU-IRT is a multifunctional icing research tunnel with a transparent test section of 0.40 m × 0.40 m × 2.0 m in size. An axial fan was used to drive the airflow cycling inside the tunnel with the wind speed in the test section up to 60 m/s. The tunnel is refrigerated via a heat exchanger, which is chilled by a 30 kW compressor (Vilter). As a result, the airflow inside ISU-IRT can be cooled down to −25 °C. An array of 8 pneumatic atomizing spray nozzles (Spraying Systems Co., 1/8NPT-SU11) along with pressure regulators were installed at the entrance of the contraction section of ISU-IRT to inject micro-sized water droplets (i.e., MVD = ~20 μm) into the airflow. The volume flow rate of water injected into the tunnel was monitored with a digital flow meter (Omega, FLR-1605A). By manipulating the pressure regulators on the air and water lines of the spray nozzles, the mass flow rate of water injected into the airflow, thereby, the liquid water content (LWC) of the airflow inside the tunnel, can be adjusted. In summary, ISU-IRT can be operated over a range of test conditions, i.e., from very dry rime ice (e.g., LWC ≈ 0.1 g/m^3) to extremely wet glaze ice (LWC > 5.0 g/m^3), to duplicate/simulate aircraft icing phenomena over a range of icing conditions.

In the present study, a NACA0012 airfoil/wing model with a chord length C = 150 mm was used for the experimental study. The airfoil/wing model was 3D printed by using a rapid prototyping machine (i.e., 3D printer). The surface of the wing model was coated with several layers of spray-on primer. The primed surfaces were then wet-sanded by using fine sandpapers (i.e., up to 2000 grit) to achieve a very smooth, glossy finish with a characteristic roughness over the surface about 25 μm. Then, a readily available all-weather protective spray-on enamel (Rustoleum, Flat Protective Enamel, white in color) was coated onto the primed surface. The sanded primer layers would provide a strong adhesion of the enamel onto the airfoil/wing surface. Supported by a stainless-steel rod, the airfoil/wing model was mounted at its quarter-chord and oriented horizontally across the middle of the test section of ISU-IRT. The angle of attack of the airfoil/wing model was adjustable by pivoting the model about the rod and fixing it at the desired angle measured with a digital inclinometer. During the experiments, the angle of attack of the airfoil/wing model was set at $\alpha = -5.0°$ in order to observe the icing and heat transfer processes on the pressure side of the airfoil/wing model, where the surface water runback and ice formation are most prominent.

As shown schematically in Fig. 2, a circular infrared (IR) transmission window of 101.6 mm in diameter (FLIR-IRW-4C) was mounted on the top panel of the ISU-IRT test section. An IR thermal imaging system (FLIR-A615 with 640 pixels × 480 pixels in spatial resolution) was mounted above the IR transmission window to map the temperature distribution over the airfoil surface during dynamic ice accreting process. The IR thermal imaging system adopts a new interface standard of GigE Vision that allows for fast image transfer to achieve 16-bit thermal imaging outputs at frame rates up to 200 Hz. In the present study, the IR thermal imaging camera was mounted at a distance of 350 mm above the airfoil/wing model. The IR radiation from the ice accreting airfoil/wing surface would be transmitted through the IR window with a transmission coefficient of 0.82. Table 1 gives the IR emissivity coefficients of the different materials, i.e., airfoil/wing model surface, ice, and liquid water, respectively.

Before performing surface temperature measurements to quantify the dynamic ice accretion process over the airfoil/wing model surface, a calibration experiment was conducted to calibrate/validate the IR thermal imaging system for the surface temperature measurements of the airfoil/wing model at several pre-scribed low temperatures (i.e., ranged from −11 °C to 0 °C). With the airfoil/wing model mounted in a calibration camber at the pre-selected temperatures, the IR thermal imaging system was used to measure the surface temperatures over the airfoil/wing model. The measurement results of the IR thermal imaging system were compared quantitatively with the nominal temperatures of the calibration camber measured by using K-typed thermocouples. A very good agreement (i.e., difference less than ±0.2 °C) was found between the nominal temperature and the measurement results of the IR thermal imaging system.

After carefully calibrated and validated, the IR thermal imaging system was then used to measure the surface temperature distributions over the ice accreting surface of the airfoil/wing model under different icing conditions (i.e., with different freestream airflow temperature T_∞, wind speed V_∞, and *LWC* levels). During the experiments, the temperatures of the incoming airflow and the surface temperature of the airfoil/wing model were also monitored by using thermocouple probes. The IR thermal imaging system was synchronized with the electric switch of the water spray system of ISU-IRT so that the dynamic ice accreting process (i.e., initial droplet impingement, transient water film/rivulets runback, and dynamic ice accretion process) over the surface of the airfoil/wing

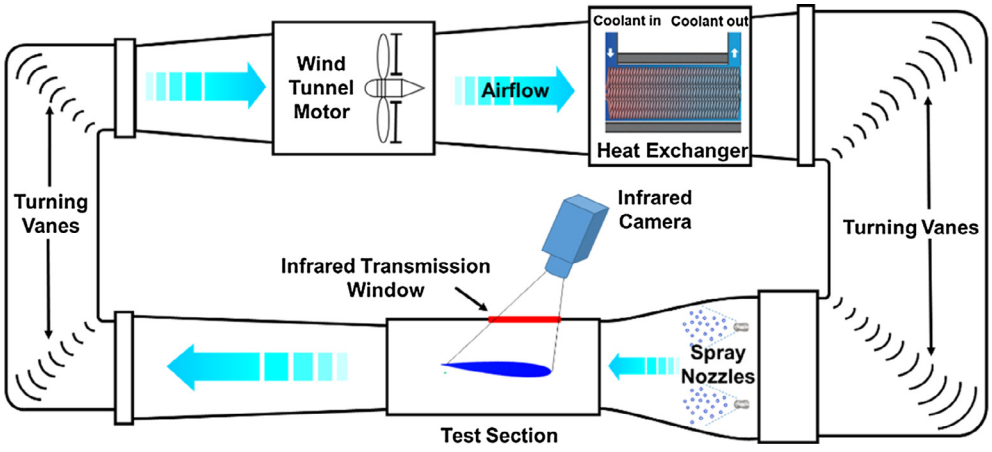

Fig. 2. A Schematic of the Icing Research Tunnel (ISU-IRT) and the experimental setup used for temperature measurements over the ice accreting airfoil/wing surface.

Table 1
Emissivity of the materials pertinent to the test model used in the present study.

Material	Emissivity
Airfoil surface (Enamel coated)	0.960
Ice	0.965
Water	0.950–0.963

model can be revealed clearly and quantitatively from the measurement results of the IR thermal imaging system.

4. Measurement results and discussions

4.1. Time evolutions of the temperature distribution over the ice accreting airfoil surface

In performing the ice accretion experiments, ISU-IRT was operated at a pre-scribed frozen-cold temperature level (e.g., $T_\infty = -8$ °C for the present study) for at least 20 min to ensure ISU-IRT reaching a thermal steady state. Since the temperature inside the ISU-IRT was set to be well below the water frozen temperature, the water droplets exhausted from the spray nozzles would be in a super-cooled state after the water spray system of the ISU-IRT was switched on at the time of $t = t_0$. Dynamic ice accretion process would start upon the impact of the super-cooled water droplets onto the surface of the airfoil/wing model.

As described above, a high-speed IR thermal imaging system was used to achieve time-resolved measurements of the surface temperature distribution over the ice accreting surface of the airfoil/wing model under different test conditions (i.e., under both dry rime icing and wet glaze icing conditions). Figs. 3 and 4 show typical snapshots of the IR measurement results over the pressure side surface of the airfoil/wing model with the incoming airflow velocity being $V_\infty = 40$ m/s, the airflow temperature $T_\infty = -8$ °C, and the liquid water content (LWC) level of the incoming airflow at $LWC = 0.3$ g/m^3 and $LWC = 3.0$ g/m^3, respectively. Based on the time sequences of the measured temperature distributions over the ice accreting airfoil surface, the characteristics of the unsteady heat transfer over the airfoil surface can be revealed clearly and quantitatively in the course of rime and glaze ice accretion processes.

As described in Papadakis et al. [32], the direct impingement area of the water droplets would concentrate within a narrow region near the stagnation line of the NACA0012 airfoil model. Due to the release of the latent heat of fusion associated with the

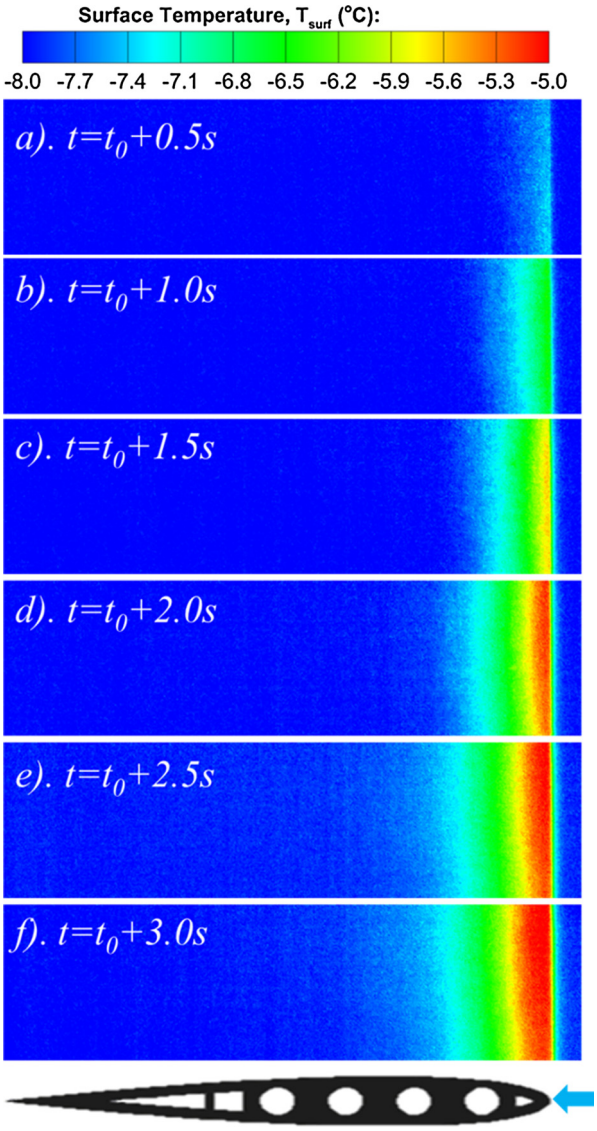

Fig. 3. Time evolution of the temperature distributions over the pressure side surface of the airfoil/wing model at AOA = −5° with the test conditions of $V_\infty = 40$ m/s, $T_\infty = -8$ °C, $LWC = 0.3$ g/m^3.

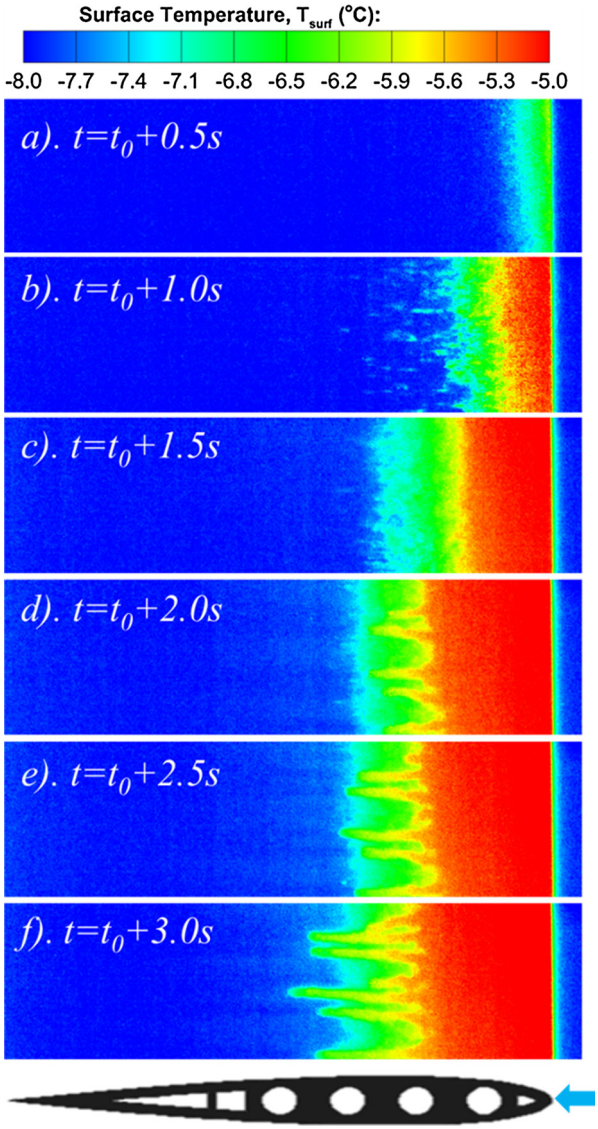

Fig. 4. Time evolution of the temperature distributions over the pressure side surface of the airfoil/wing model at AOA = −5° with the test conditions of V_∞ = 40 m/s, T_∞ = −8 °C, LWC = 3.0 g/m^3.

solidification of the impinged super-cooled water droplets (i.e., icing process), the temperature within the impingement area of the water droplets would increase rapidly. As shown clearly in Fig. 3(a), with the very first group of the super-cooled water droplets impacted onto the airfoil surface (i.e., at the time instance of $t = t_0 + 0.5$ s), the surface temperature within the direct impingement area of the super-cooled water droplets (i.e., the narrow region near the airfoil leading edge) was found to increase rapidly due to the release of the latent heat of fusion associated with the icing process, as expected. It should be noted that, even though the surface temperature near the airfoil leading edge was found to become higher than the ambient temperature (i.e., $T_{surface} > -8$ °C), their values were found to be still much lower than the water frozen temperature for both of the test cases, indicating that the water droplets were in a super-cooled state before impinged onto the airfoil surface. As described in Davis [33] and further confirmed by Jung et al. [34], there are two sequential stages in the course of the freezing process for a super-cooled water droplet. At the first stage, a partial solidification of the super-cooled water droplet would take place very rapidly, with most of the released latent heat of fusion being absorbed by the remaining liquid water to cause its temperature increase, while only a small portion of the heat would be transferred to the surroundings. In the second stage, the remaining liquid water would freeze isothermally at a much slower rate (i.e., nearly three orders of magnitude slower than the first stage, as described in Jung et al. [34]). The freezing process in the second stage would be mainly controlled by the rate of heat transfer through convection or conduction, resulting in a freezing front at either the gas-liquid or liquid-solid interface. As a result, upon impingement of the super-cooled water droplets onto the airfoil surface, the icing process can be either finished completely or partially, depending on how rapidly the released latent heat of fusion can be transferred and/or dissipated into the surrounding ambient.

For the test case as that given in Fig. 3, with the incoming airflow being quite dry (i.e., LWC = 0.3 g/m^3) at relatively low temperature (i.e., $T_{air,\infty} = -8$ °C), the super-cooled water droplets carried by the incoming airflow would freeze immediately upon impact onto the surface of the airfoil/wing model. As described in Hansman and Kirby [2], with the ambient temperature being far below the water freezing point, the heat transfer would be sufficiently strong to rapidly remove all of the released latent heat of fusion. As a result, the icing morphology over the surface of the airfoil/wing model was found to be of typical rime ice accretion process, and no surface water runback was observed for this test case. It is called dry ice growth process by Hansman and Kirby [2]. As shown clearly in Fig. 3, right after the very first group of the super-cooled water droplets impinged onto the airfoil surface near the leading edge (i.e., at the initial stage of ice accretion during the time instances from $t = t_0$ to $t = t_0 + 0.50$ s), the latent heat of fusion was rapidly released to cause the surface temperature near the stagnation line to increase instantly. The strong convective heat transfer was found to remove the heat from the remaining liquid water very quickly, resulting in an immediate frozen of the entire impinged liquid water mass with its temperature decreased to the same level as the ambient airflow (i.e., $T_{air,\infty} = -8$ °C) rapidly. As the time goes on, due to the continuous impingement of the super-cooled water droplets onto the airfoil surface, the ice layer accreted near the airfoil leading edge was found to become thicker and thicker. As revealed clearly from the measured temperature distributions during the time instances from $t = t_0 + 1.5$ s to $t = t_0 + 3.0$ s, the regions with relatively higher surface temperature (i.e., due to the greater amount of latent heat release) were still found to concentrate within a narrow area near the airfoil stagnation line for this rime ice accretion case.

As described in Potapczuk [1], rime ice accretion occurs mainly in the impingement region, which would closely follow the original contour of the airfoil profile [1]. Papadakis et al. [32] reported that, while the maximum water collection efficiency would occur at the stagnation point of the airfoil, the water collection efficiency would decrease very quickly and become almost zero in the region far away from the stagnation point. As shown clearly in Fig. 3, the regions with relatively high temperatures were found to concentrate within the direct impingement region of super-cooled water droplets, and the temperature decreased rapidly in the region far away from the leading edge. Such distribution pattern in the measured surface temperature maps was found to be in good accordance with the typical water collection efficiency distribution for the NACA0012 airfoil/wing model.

As shown clearly in Fig. 4, with the velocity and temperature of the incoming airflow being still kept at the same values of $V_{air,\infty}$ = 40 m/s and $T_{air,\infty} = -8$ °C, but the incoming airflow being quite wet with LWC = 3.0 g/m^3, the ice accreting process over the airfoil/wing surface was found to become of typical glaze ice accretion, which is significantly different from the rime ice accretion process shown in Fig. 3. In comparison with the rime ice accretion case described above, since the LWC value was increased by a factor of 10 for this

test case, much more super-cooled water droplets would impinge onto the airfoil surface within the same time duration after the spray system of ISU-IRT was switched on. As a result, the airfoil surface was found to become wetted very rapidly. Upon impact of the 10 times more water mass onto the airfoil surface, a much greater amount of the latent heat of fusion would be released within the same duration. As shown clearly in Fig. 4(a), right after the spray system of ISU-IRT was turned on (i.e., at the time instance of $t = t_0 + 0.5$), the temperature distribution over the airfoil surface was found to have a similar pattern as the droplet impingement efficiency distribution as reported in Papadakis et al. [32], i.e., with the maximum occurring at the stagnation region and decreasing rapidly at further downstream locations. As described in Jung et al. [34], the released latent heat of fusion would be absorbed by the liquid water at first to cause its temperature to increase rapidly, and then the released latent heat was transferred/dissipated to surroundings via convection and/or conduction in a much slower rate. Due to the continuous impingement of the massive super-cooled water droplets carried by the incoming airflow onto the airfoil surface, more and more latent heat of fusion would be released, causing a greater surface temperature increase over the ice accreting airfoils, as shown in Fig. 4(b). The heat transfer process, however, was not fast enough to remove all the latent heat of fusion from the impinged water mass for this test case, and caused a portion of the impinged water mass to stay in liquid phase to form a water film over the airfoil surface. Driven by the boundary layer airflow over the airfoil surface, the unfrozen water film would run back along the airfoil surface and then freeze at further downstream in the region beyond the direct impingement area of the super-cooled water droplets, as can be seen clearly from the measured temperature map at the time instance of $t = t_0 + 1.5$ s shown in Fig. 4(c). As revealed clearly in Zhang et al. [35] and Liu et al. [36], due to the complex interactions among the multiphase flows (i.e., boundary layer airflow, unfrozen liquid water in either droplet or film morphology, and the accreted solid ice over the airfoil surface), the front contact line of the water film over the airfoil surface would break up to form finger-like structures (i.e., rivulet structures) as the surface water ran back, which were revealed clearly from the measurement results given in Fig. 4(d), (e) and (f). Similar phenomena were also observed in the experimental studies of Hansman [37] and Waldman and Hu [38]. Such finger-like rivulet structures would serve as the water runback channels to transport the continuously impinged unfrozen water mass from the airfoil leading edge to downstream regions. Along with the runback of the unfrozen water mass over the airfoil surface, a large amount of released latent heat of fusion would also be transported downstream through the rivulets, as indicated by the higher temperature stripes in the measured temperature maps at the time instances of $t = t_0 + 2.0$ s to $t = t_0 + 3.0$ s (i.e., as shown in Fig. 4(d), (e) and (f)). As the unfrozen water ran back over the airfoil surface, the heat stored in the liquid water would be transferred/dissipated to the surroundings mostly by convection. Since the ambient temperature during the experiment was well below the frozen temperature of water (i.e., $T_{air,\infty} = -8$ °C), the runback water would be frozen into ice eventually to from rivulet-shaped ice features over the airfoil/wing surface, as reported in Waldman and Hu [38].

Based on the time sequences of the acquired IR thermal images as those shown in Figs. 3 and 4, the variations of the temperature at the selected points over the surface of the airfoil/wing model can be extracted quantitatively for further analysis. Fig. 5 shows the time evolutions of the temperature increment (i.e., $\Delta T = T_{surface} - T_{air,\ \infty}$) at five typical chord-wise positions over the airfoil/wing surface under different icing test conditions (i.e., rime ice vs. glaze ice accretion), which can be used to reveal the characteristics of the ice accreting processes more clearly and quantitatively. The locations of the five pre-selected points were shown schematically in Fig. 5(a). While the first point (i.e., point A) was selected to be at the airfoil leading edge in the middle span of the airfoil/wing model, the other four points (i.e., the points of B, C, D, and E) were also located in the middle plane of the airfoil/wing model, spreading along the chord-wise direction with the same spacing of 10% chord length.

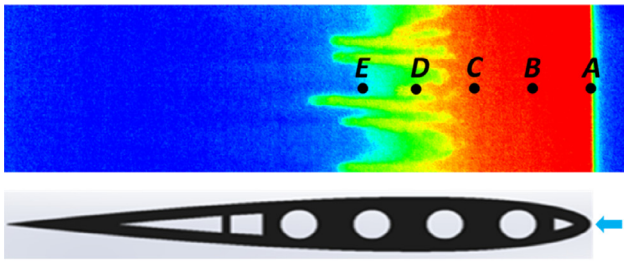

(a). Location of the 5 selected points

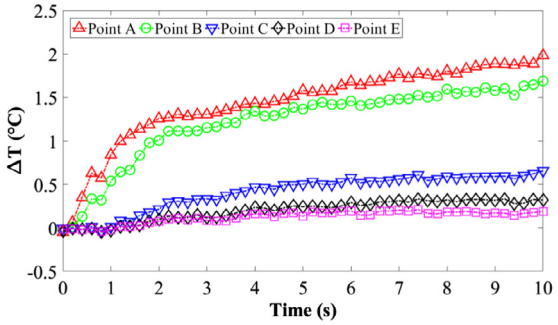

(b). the test case with $LWC = 0.3$ g/m^3

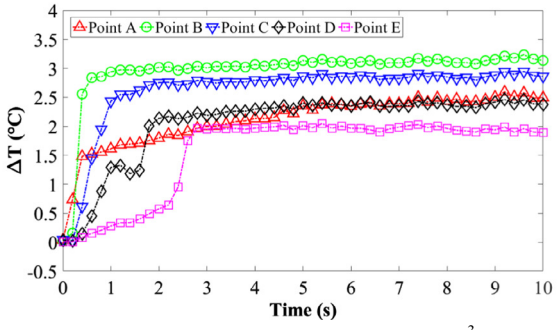

(c). the test case with $LWC = 3.0$ g/m^3

Fig. 5. Time evolution of the measured temperature increments at 5 selected chord-wise locations over the ice accreting airfoil surface under the icing test condition of $V_{air,\infty} = 40$ m/s and $T_{air,\infty} = -8$ °C; but with the *LWC* being of 0.3, and 3.0 g/m^3, respectively.

As described above, under the icing test conditions of $V_{air,\infty} = 40$ m/s and $T_{air,\infty} = -8$ °C, the ice accreting process over the airfoil/wing surface would be of typical rime ice accretion when the *LWC* level of the incoming airflow being relatively low (i.e., at $LWC = 0.3$ g/m^3). Due to the almost immediate freezing of the super-cooled water droplets upon impact onto the airfoil surface for such a dry ice accreting process, all the water mass collected over the airfoil surface would freeze immediately to form rime ice within the direct impingement area of the super-cooled water droplets (i.e., within a narrow region near the airfoil stagnation line). Corresponding to the higher water collection efficiency near the stagnation point as reported in Papadakis et al. [32], only the temperature values at point A (i.e., the airfoil leading edge) and point B (i.e., 10% chord length downstream) were found to increase rapidly as the icing test experiment just started (i.e., $t < 1.5$ s), while the temperatures at other downstream points were found to be almost unchanged, especially for those points beyond the

direct impingement region of the super-cooled water droplets (i.e., the points of C, D and E), as shown clearly in Fig. 5(b). As the time goes on, with the continuous impingement of the super-cooled water droplets on the ice accreting airfoil surface, the temperature within the direct impingement region was found to keep increasing, but with a much slower increasing rate, indicating a thermal equilibrium state would be achieved over the ice accreting airfoil. For the temperature evolution at point C (i.e., 20% chord length downstream), since it is located at the far edge of the direct impingement region as reported in Papadakis et al. [32], only a very limited amount of the super-cooled water droplets can reach the downstream location and froze subsequently. As the time goes on, only a small temperature increase (i.e., ~0.5 °C) was observed as shown in Fig. 5(b). During the ice accretion process, while the released latent heat of fusion within the direct impingement region are expected to be mostly taken away by convective heat transfer via the boundary layer airflow over the airfoil surface, a small portion of the released latent heat of fusion may also dissipate within the airfoil/wing substrate via heat conduction. Both the convective and conductive heat transfer may cause the slight temperature increases over the downstream airfoil surface beyond the direct impingement region, as can be seen at the point D and E (i.e., 30% and 40% chord length downstream of the airfoil leading edge).

For the test case with the LWC level in the incoming airflow being increased to $LWC = 3.0$ g/m^3, much more super-cooled water droplets (i.e., by a factor of 10) would impinge onto the airfoil surface within the same time duration of the experiment. As revealed clearly in Fig. 5(c), due to the significant amount of the water mass collected around the airfoil leading edge for such a wet test case, the heat transfer process was not fast enough to remove all the released latent heat of fusion. As a result, only a portion of the impacted water mass would be frozen into ice upon impact, and the rest of the impinged water mass remained in liquid state. As driven by the boundary layer airflow over the airfoil surface, the unfrozen liquid water would run back along the airfoil surface. As shown clearly in Fig. 5(c), at the beginning of the icing experiment (i.e., $t < 1.5$ s), the surface temperature was found to increase rapidly not only within the direct impingement region of the super-cooled water droplets (i.e., at the points of A and B), but also at the further downstream location (i.e. at the points of C and D, which are beyond 20% chord length). Interestingly, the temperature increments at the locations of 10% and 20% chord length downstream (i.e., at the points of B and C) were found to become even greater than that at the leading edge (i.e., at the point A) very soon after the ice accretion experiment started (i.e., less than $t = 1.0$ s). It was suggested that such a shift in the maximum temperature increment was due to the obvious runback of the unfrozen water over the airfoil surface. As the time goes on, with the continuous impingement of the super-cooled water droplets onto the airfoil surface, the unfrozen liquid water would form film/rivulet flow to transport the impacted water mass into the further downstream locations. Due to the release of the latent heat release associated with the solidification of the runback surface water over the airfoil surface, the temperatures at the point D and E (i.e., at the downstream locations of 30% and 40% chord length) were also found to increase substantially at the time instants of $t = 2.0$ s and $t = 3.0$ s, as shown in Fig. 5(c). As the time goes by, a thermal equilibrium state was found to achieve along the ice accreting airfoil surface. As a result, the temperature increments over the ice accreting airfoil surface were found to become almost unchanged after $t = 3.0$ s, as shown clearly in Fig. 5(c).

It should be noted that, a greater temperature increment at a location would indicate more latent heat of fusion released due to the solidification of the liquid water, hence, more ice accretion at the downstream location. The measured temperature results given in Fig. 5 also suggest that, in comparison with that at the airfoil leading edge, a greater amount of ice would be accreted at the downstream locations of 10% and 20% chord length for this glaze ice accretion case, which was confirmed by measuring the ice morphology accreted over the surface of the airfoil/wing model after finishing the ice accretion experiment. Similar findings were also reported in the experimental study of Waldman and Hu [38], in which a high-speed imaging system was used to quantify the transient glaze ice accretion process over a similar airfoil/wing model as that used in the present study.

4.2. Further discussions about the temperature distributions near the airfoil leading edge

As described above about theoretic analysis of convective heat transfer over the surface of the ice accreting airfoil, water collection efficiency (β) is a very important parameter that needs to be quantitatively defined. The measured surface temperature distributions given in Figs. 3 and 4 reveal clearly that, at the initial stage of ice accreting process, the temperature gradients around the airfoil leading edge would comply well with the variations of droplet impingement intensity as described in Papadakis [32] and Özgen and Canıbek [39]. Therefore, in the present study, an effort was made to quantitatively define the distribution of water collection efficiency based on the time-resolved temperature measurements around the airfoil leading edge.

Fig. 6 shows the time-evolutions of the surface temperature increments around the leading edge of the ice accreting airfoil with the freestream velocity and temperature being $V_{air,\infty} = 40$ m/s and $T_{air,\infty} = -8$ °C, while the LWC levels being 0.3 g/m^3 to 3.0 g/m^3,

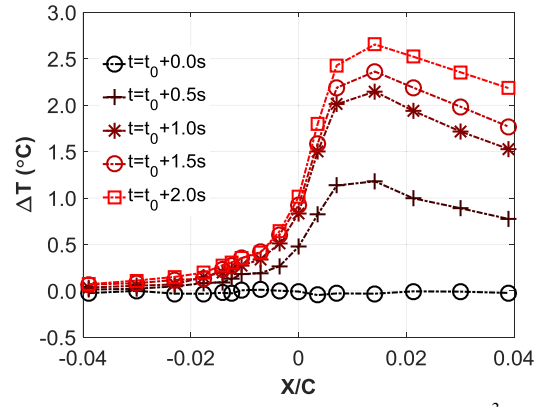

(a). the test case with $LWC = 0.3$ g/m^3

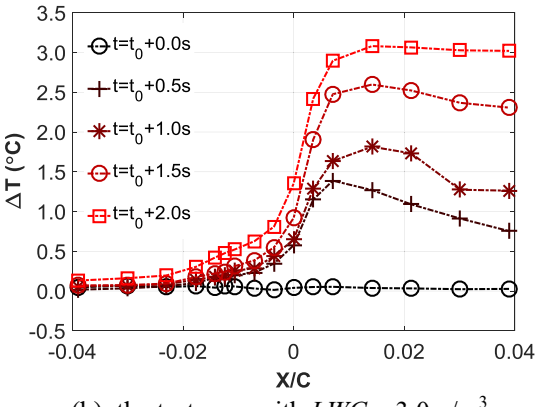

(b). the test case with $LWC = 3.0$ g/m^3

Fig. 6. Time-evolutions of the temperature distribution around the ice accreting airfoil leading edge with the freestream airflow velocity $V_{air,\infty} = 40$ m/s and temperature $T_{air,\infty} = -8$ °C. (a) $LWC = 0.3$ g/m^3. (b) $LWC = 3.0$ g/m^3.

respectively. As discussed above, for the test case of LWC = 0.3 g/m^3, the ice accretion process over the airfoil/wing surface is a typical rime icing process, with the impinged super-cooled water droplets being frozen immediately upon impact. Therefore, a greater temperature increment over the airfoil surface for this test case would indicate directly more latent heat release due to the solidification of the impinged liquid water mass, thereby, more ice accretion at the location. As shown clearly in Fig. 6(a), before the super-cooled water droplets impinged onto the airfoil surface, the surface temperature around the airfoil leading edge was found to be the same as the incoming airflow temperature, i.e., with zero temperature increment, as expected. After the super-cooled water droplets impinged onto the airfoil surface (i.e., at the time instant of $t = t_0 + 0.5$ s), due to the release of the latent heat of fusion associated with the solidification of the impacted super-cooled water droplets, the measured surface temperatures around the airfoil leading edge (i.e., from $X/C = 0$ to $X/C = 0.04$) were found to increase rapidly with a similar pattern as that of the water collection efficiency given in Papadakis [32] and Özgen and Canıbek [39]. It was found that the maximum temperature increment was located at $X/C \approx 0.014$, which was the stagnation point when the attack of angle of the airfoil/wing model was set at $\alpha = -5°$ for the present study. As the time goes on, with more and more super-cooled water droplets impinging onto the airfoil surface, the ice layer accreted over that airfoil surface within the direct impingement region of the super-cooled water droplets would become thicker and thicker, as indicated by the continuous temperature increase around the airfoil leading-edge from the time instant of $t = t_0 + 0.5$ s to $t = t_0 + 2.0$ s. It should be noted that, in such a dry rime ice accretion process, the total amount of the ice accumulation at a location over the airfoil surface would be solely determined by the local water collection efficiency. Therefore, by measuring the temperature increments over the airfoil surface that is linearly proportional to the total amount of released latent heat of fusion due to the solidification of the impacted super-cooled water droplets, the distribution of the water collection efficiency over the airfoil surface can be determined quantitatively during the rime ice accretion process.

When the LWC level in the incoming airflow was increased to LWC = 3.0 g/m^3, 10 times more super-cooled water droplets would impinge onto the airfoil surface within the same time duration of the ice accretion experiment. As shown clearly in Fig. 6(b), with the very first group of the super-cooled water droplets impinged onto the airfoil surface (i.e., at the time instance of $t = t_0 + 0.5$ s), a very similar temperature distribution over the airfoil surface for this wet glaze ice accretion case was observed as that of the dry rime ice accretion case described above, due to the rapid release of the latent heat of fusion upon the impact of the super-cooled water droplets [33]. However, as the time goes by, associated with the more and more super-cooled water impinged onto the airfoil surface, the much larger amount of the latent heat of fusion released during the same time duration could not be transferred out and/or dissipated rapidly for this test case. As a result, a significant portion of the released latent heat absorbed by the unfrozen liquid water would be transported downstream along with the surface water runback, as driven by the boundary layer airflow. Therefore, the distribution of the temperature increments around the airfoil leading edge would be no longer determined solely by the local water collection efficiency. As shown clearly in Fig. 6(b), a much more uniform temperature pattern was observed in the region of $X/C = 0.014$ to $X/C = 0.04$ at the ice accretion time of $t > t_0 + 1.0$ s.

As discussed above, for the dry rime ice accretion case, the distribution of water collection efficiency of the airfoil/wing model can be determined quantitatively based on the analogy between the distributions of the measured temperature increment and the water collection efficiency around the airfoil surface. In the present study, the normalized water collection efficiency, i.e., the ratio of the local water collection efficiency to the maximum water collection efficiency at the stagnation point, is defined as:

$$\overline{\beta_i} = \beta_i/\beta_0 \tag{21}$$

where β_i is the local water collection efficiency, and β_0 is the water collection efficiency at the stagnation point.

For the dry rime ice accretion case, since the measured temperature increment around the airfoil surface is proportional to the local water collection efficiency (i.e., $\Delta T_i \propto \beta_i$), the normalized water collection efficiency over the airfoil surface can be estimated directly based on the measured surface temperature distributions shown in Fig. 6(a), i.e., $\overline{\beta_i}=\beta_i/\beta_0 = \Delta T_i/\Delta T_0$, where ΔT_i is the local temperature increment, and ΔT_0 is the temperature increment at the stagnation point of the airfoil/wing model. By scaling the chord-wise coordinates (i.e., $X/X_{\beta 0}$, where $X_{\beta 0}$ is the airfoil stagnation point), distributions of the normalized water collection efficiency at the different time instances (i.e., $t = t_0 + 0.5$ s, $t = t_0 + 1.0$ s, $t = t_0 + 1.5$ s, and $t = t_0 + 2.0$ s) were calculated and plotted in Fig. 7. The predictions of the water collection efficiency for a NACA0012 airfoil/wing model at the angle of attack of AOA = 5.0° (i.e., with a mirrored distribution curve of that at AOA = −5.0°) by using the theoretical model suggested by Özgen and Canıbek [39] were also given in the same plot for quantitative comparison.

As shown clearly in Fig. 7, the normalized water collection efficiency data calculated based on the measured temperature increments of the present study agree well with the predictions of the theoretic model suggested by Özgen and Canıbek [39] in general, which validates the method of the present study to determine the water collection efficiency profile of the airfoil/wing model by measuring the surface temperature distributions over the airfoil/wing surface during the dynamic rime ice accreting process.

By comparing the measurement data obtained at the different instances after starting the rime ice accretion experiment, it can be seen clearly that, while the normalized water collection efficiency data in the region near the airfoil stagnation point (i.e., $0 < X/X_{\beta 0} < 1.5$) were found to have almost no variations as the time goes by, the water collection efficiency data based on the surface temperature measurements obtained at the later time instances were found to be greater than those at the earlier time instances, especially in the downstream locations far away from the airfoil stagnation point (i.e., $X/X_{\beta 0} > 2.0$). It may be explained by the facts that, as the super-cooled water droplets impinged onto the airfoil surface in the region near the stagnation point(i.e., $X/X_{\beta 0} \approx 1$), a normal impact for the impinging water droplets is expected. Since

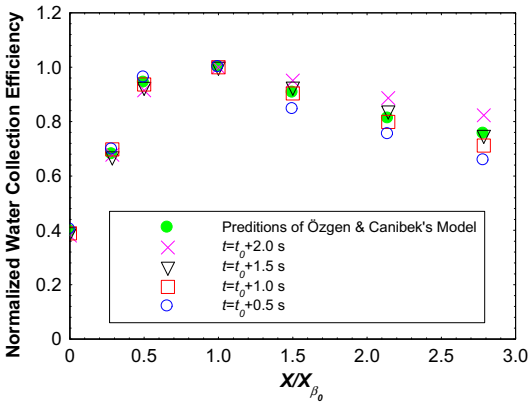

Fig. 7. Normalized water collection efficiency distributions over the airfoil surface derived from the present experimental study vs. the predictions of Özgen and Canıbek's model [39].

the super-cooled water droplets would be impinging normally onto the airfoil surface and frozen immediately upon impact due to the fast heat transfer under the dry rime ice accretion condition, the accreted ice over the airfoil surface in the region near the airfoil stagnation point (i.e., at $X/X_{\beta 0} \approx 1.0$) had almost no effects on the behaviors of the normally impact water droplets, the water collection efficiency in the region would be at almost the same values, as the time goes by.

However, as the water droplets impinged onto the airfoil surface in the region far away from the airfoil stagnation point ($X/X_{\beta 0} > 1.5$), an oblique impact process is expected for the impinging water droplets [40]. As the time goes by, with more and more super-cooled water droplets impacting on the airfoil surface in the region, the thicker and thicker ice layer accreted over the airfoil surface would grow outwards into the incoming airflow to catch more super-cooled droplets carried by the incoming airflow. As a result, the water collection efficiency in the downstream region far away from the airfoil stagnation point (i.e., in the downstream region of $X/X_{\beta 0} > 1.5$) is expected to increase continuously as the time goes by. As shown clearly in Fig. 7, with the ice accretion time increasing from $t = t_0 + 0.5$ s to $t = t_0 + 2.0$ s, the values of the water collection efficiency at the downstream locations of $X/X_{\beta 0} > 1.5$ were found to increase noticeably (i.e., was found to increase by 12.4% at the downstream location of $X/X_{\beta 0} = 1.5$, and by an even greater factor of 25.3% at the further downstream location of $X/X_{\beta 0} = 2.8$).

For the dry rime ice accretion case, since the super-cooled water droplets would freeze immediately upon impact, the local freezing fraction is expected to be unity around the airfoil leading edge with no surface water runback. Thus, the expression of the convective heat transfer coefficient given in Eq. (20) can be reduced as:

$$h_{cv} = \frac{[\Delta T/R_{cond,tot} - LWC \cdot V_{imp} \cdot \beta[L_s + (T_f - T_{surf}) \cdot C_i] - 0.5 \cdot LWC \cdot V_{imp}^3]}{[T_{rec} - T_{air,\infty} - \Delta T - 0.696 \cdot [p_s(T_b) - p_s(T_{air,\infty})]/(C_a \cdot p_m) \cdot L_i]} \tag{22}$$

In this reduced form of convective heat transfer coefficient, the temperature difference, ΔT, has been quantitatively measured. Combined with the distribution of water collection efficiency derived in the present study and the previously defined relevant parameters [6,27–32,39], the local convective heat transfer coefficient around the airfoil leading edge can be calculated. In the present study, the Frossling number was used to represent the variation in the convective heat transfer coefficient as suggested by Dukhan et al. [41] and Poinsatte et al. [42]. The Frossling number can be calculated by

$$Fr = NuRe^{-0.5} = (h_{cv}c/k)(Vc/\upsilon)^{-0.5} \tag{23}$$

where c is the chord length of the airfoil, k is the thermal conductivity of air, V is the freestream velocity, and υ is the kinematic viscosity of airflow.

Fig. 8 shows the time evolution of the measured Frossling numbers around the airfoil leading edge of the present study during the rime ice accretion process, i.e., with the incoming airflow velocity being $V_{air,\infty} = 40$ m/s, the temperature being $T_{air,\infty} = -8$ °C, and the liquid water content (LWC) being $LWC = 0.3$ g/m^3. The measured Frossling numbers of a previous study of Newton et al. [43] were also plotted in Fig. 8 for comparison, in which the heat transfer measurements were performed over the smooth surface of a NACA0012 airfoil model at the same angle of attack (i.e., $\alpha = -5°$). As shown in Fig. 8, the distributions of the measured Frossling number around the airfoil leading edge for the present study were found to follow the same trend as that given in Newton et al. [43]. According to the heat transfer textbook of Incropera and DeWitt [27], the convective heat transfer over the airfoil surface would be influenced greatly by the boundary layer airflow over the airfoil surface. As shown clearly in Fig. 8, while the rate of the convective heat transfer was found to be at its peak at the airfoil stagnation point (i.e., having the maximum value for the Frossling numbers), the measured Frossling numbers were found to decrease gradually at the downstream locations away from the airfoil stagnation point due to the development of the boundary layer and acceleration of the airflow over the airfoil surface.

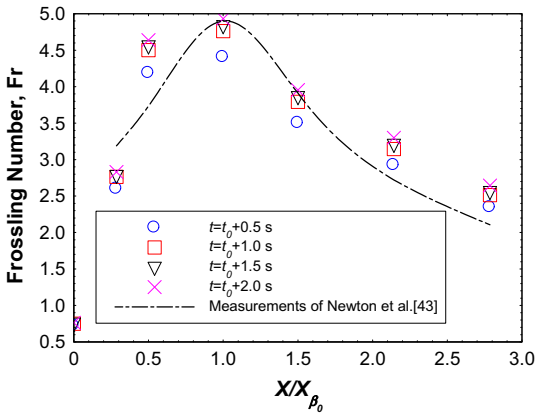

Fig. 8. The time evolution of the measured Frossling numbers of the present study vs. the measurement results of Newton et al. [43].

As described above, for the present rime ice accretion case, the super-cooled water droplets carried by the incoming airflow would freeze instantly upon impact onto the airfoil surface, forming ice roughness within the direct impingement region near the airfoil leading edge [44]. The formation of such ice roughness near the airfoil leading edge would greatly promote the growth and transition of the laminar boundary layer airflow over the airfoil surface, thereby, enhancing the convective heat transfer process over the airfoil surface [41,45]. As the time goes by, with more and more super-cooled water droplets impinging onto the airfoil surface and proceed the rime ice accretion process, the airfoil surface would become rougher and rougher. Therefore, as shown quantitatively in Fig. 8, the Frossling numbers over the airfoil surface were found to increase continuously as the ice accretion time increases. More specifically, at the very beginning of the ice accretion process, i.e., at the time instance of $t = t_0 + 0.5$ s, the Frossling numbers at the airfoil stagnation point (i.e., at $X/X_{\beta 0} = 1$, where $X_{\beta 0}/C = 0.014$) and the downstream location of $X/X_{\beta 0} = 2.8$ were found to be $Fr \approx 4.4$ and $Fr = 2.3$, respectively. As the ice accretion time increase to $t = t_0 + 2.0$ s, with much more super-cooled water droplets impinged onto the airfoil surface to form ice roughness over the airfoil surface, the corresponding Frossling numbers were found to increase to $Fr = 4.9$ (i.e., ∼11% increase) at the stagnation point, and $Fr = 2.6$ (i.e., ∼13% increase) at the downstream location of $X/X_{\beta 0} = 2.8$. The findings derived from the present study suggest that, in the course of the ice accretion process, the convective heat transfer over the airfoil surface would be enhanced substantially due to the formation of the ice roughness over the airfoil surface. Such enhanced convective heat transfer would further promote the ice formation and accretion over the airfoil surface as more and more super-cooled water droplets impact onto the roughed airfoil surface.

5. Conclusion

In the present study, an experimental investigation was performed to examine the unsteady heat transfer and dynamic ice accretion processes over the surface of a NACA 0012 airfoil/wing

model under different icing conditions. The experiments were conducted in the unique Icing Research Tunnel available at Iowa State University (i.e., ISU-IRT). During the experiments, while the freestream velocity and temperature of the airflow in ISU-IRT were kept at $V_{air,\infty}$ = 40 m/s and $T_{air,\infty}$ = −8 °C, the liquid water content (*LWC*) level of the airflow was changed from *LWC* = 0.3 g/m^3 to *LWC* = 3.0 g/m^3 in order to generate typical dry rime icing and wet glaze icing conditions. A high-speed Infrared (IR) thermal imaging system was used to achieve time-resolved temperature distribution measurements to quantify the unsteady heat transfer and dynamic phase changing process over the ice accreting airfoil/wing surface under different icing conditions (i.e., dry rime icing vs. wet glaze icing). In the present study, a theoretic heat transfer model was also developed as a function of the key test parameters (e.g., *LWC*, freestream velocity and temperature of the airflow, water collection distribution, and local freezing fraction) to characterize the unsteady heat transfer process over the ice accreting airfoil/wing surface.

The measurement results reveal clearly that, under both dry rime and wet glaze icing conditions, the direct impingement area of the super-cooled water droplets would concentrate mainly within a narrow region near the stagnation point of the airfoil/wing model. With the LWC level of the airflow in ISU-IRT being relatively small (i.e., *LWC* = 0.3 g/m^3), the heat transfer process was found to be sufficiently fast to remove all the latent heat of fusion released during the solidification process of the impinged super-cooled water droplets, resulting in typical rime ice accretion scenario over the airfoil surface. As the time goes by, with more and more super-cooled water droplets impinging onto the airfoil surface, while the ice layer accreted over the airfoil surface was found to become thicker and thicker, a thermal equilibrium state was found to be reached eventually with the surface temperatures of the airfoil/wing model being almost constant as the ice accretion process goes on.

When the *LWC* level of the incoming airflow was increased to LWC = 3.0 g/m^3, due to the insufficient heat transfer to remove all the released latent heat of fusion associated with the solidification of the much more impinged super-cooled water mass over the airfoil surface, the ice accretion was found to become of a typical glaze ice accretion process with significant surface water runback being observed in the form of film/rivulets morphologies. Along with the surface water runback, a great amount of the latent heat of fusion released during the solidification process was transported downstream and then transferred/dissipated by convection, forming the rivulet-shaped features in the measured surface temperature maps.

Based on the time evolution of measured surface temperature distributions over the airfoil surface for the typical dry rime ice accretion case, the distributions of the water collection efficiency over the airfoil surface were determined quantitatively based on the analogy between the surface temperature increment due to rime ice accretion and the water collection efficiency around the airfoil surface. The estimated water collection efficiency data were then imported into the theoretic heat transfer model to evaluate the unsteady heat transfer over the airfoil/wing surface during the dynamic rime ice accretion process. It was found that the convective heat transfer would reach its maximum at the airfoil stagnation point, and decrease gradually at the downstream locations due to the development of the boundary layer airflow. The formation of ice roughness near the airfoil leading edge was found to be able to greatly promote the growth and transition of the laminar boundary layer airflow over the airfoil surface, thereby, enhancing the convective heat transfer process over the airfoil surface. The enhanced convective heat transfer would further promote the ice formation and accretion over the roughed airfoil surface.

Conflict of interest

The authors declare that there are no conflicts of interest.

Acknowledgments

The work is partially supported by National Aeronautical and Space Administration (NASA) – Grant number NNX12AC21A with Mr. Mark Potapczuk as the technical officer. The support of National Science Foundation (NSF) under award numbers of CBET-1064196 and CBET-1435590 is also gratefully acknowledged.

References

[1] M.G. Potapczuk, Aircraft icing research at NASA Glenn research center, J. Aerosp. Eng. 26 (2013) 260–276.
[2] R.J. Hansman, M.S. Kirby, Comparison of wet and dry growth in artificial and flight icing conditions, J. Thermophys. Heat Transf. 1 (1987) 215–221, https://doi.org/10.2514/3.30.
[3] J. Steuernagle, K. Roy, D. Wright, Aircraft icing, in: Saf. Advis. (Weather No. 1), Air Saf. Found. Spons. by FAA, Flight Saf. Branch, 2008.
[4] T. Vasquez, Air France Flight 447: A detailed meteorological analysis, Weather Graph., 2009. <http://scholar.google.com/scholar?q=Air+France+Flight+447+&btnG=&hl=en&as_sdt=0%2C16#5> (accessed October 2, 2015).
[5] Y. Liu, L. Bond, H. Hu, Ultrasonic-attenuation-based technique for ice characterization pertinent to aircraft icing phenomena, AIAA J. 55 (5) (2017) 1602–1609, https://doi.org/10.2514/1.J055500.
[6] G. Fortin, J.-L. Laforte, A. Ilinca, Heat and mass transfer during ice accretion on aircraft wings with an improved roughness model, Int. J. Therm. Sci. 45 (2006) 595–606, https://doi.org/10.1016/j.ijthermalsci.2005.07.006.
[7] R. Hansman, S. Turnock, Investigation of surface water behavior during glaze ice accretion, J. Aircr. 26 (2) (1989) 140–147.
[8] K. Yamaguchi, R.J. Hansman, Heat transfer on accreting ice surfaces, J. Aircr. 29 (1992) 108–113.
[9] Y. Cao, S. Hou, Extension to the myers model for calculation of three-dimensional glaze icing, J. Aircr. 53 (1) (2016) 106–116.
[10] S.K. Thomas, R.P. Cassoni, C.D. MacArthur, Aircraft anti-icing and de-icing techniques and modeling, J. Aircr. 33(5) (2012) 841–854. <http://arc.aiaa.org/doi/abs/10.2514/3.47027> (accessed February 14, 2016).
[11] W.B. Wright, User manual for the NASA Glenn ice accretion code LEWICE [microform]: version 2.0/William B. Wright, National Aeronautics and Space Administration, Glenn Research Center; National Technical Information Service, distributor. Cleveland, Ohio: Springfield, Va, 1999.
[12] R. Gent, J. Ford, R. Moser, D. Miller, SLD Research in the UK, in: FAA In-Flight Icing Gr. De-Icing Int. Conf. Exhib. Chicago, Illinois, June 16–20, 2003, 2003. <http://papers.sae.org/2003-01-2128/> (accessed October 2, 2015).
[13] C. Bidwell, Icing calculations for a 3D, high-lift wing configuration, 43rd AIAA Aerosp. Sci. Meet. Exhib. 10–13 January 2005, Reno, Nevada, AIAA 2005-1244, 2005. <http://arc.aiaa.org/doi/pdf/10.2514/6.2005-1244> (accessed November 15, 2014).
[14] T.G. Myers, J.P.F. Charpin, C.P. Thompson, Slowly accreting ice due to supercooled water impacting on a cold surface, Phys. Fluids 14 (2002) 240, https://doi.org/10.1063/1.1416186.
[15] S. Campbell, A. Broeren, M. Bragg, D. Miller, Aircraft performance sensitivity to icing cloud conditions, in: 45th AIAA Aerosp. Sci. Meet. Exhib., American Institute of Aeronautics and Astronautics, Reston, Virigina, 2007. http://doi.org/10.2514/6.2007-86.
[16] R.J. Kind, M.G. Potapczuk, A. Feo, C. Golia, A.D. Shah, Experimental and computational simulation of in-flight icing phenomena, Prog. Aerosp. Sci. 34 (1998) 257–345.
[17] B.L. Messinger, Equilibrium temperature of an unheated icing surface as a function of air speed, J. Aeronaut. Sci. (Institute Aeronaut. Sci.) 20 (1953) 29–42.
[18] T.G. Myers, Extension to the Messinger model for aircraft icing, AIAA J. 39 (2001) 211–218.
[19] W. Olsen, E. Walker, Experimental Evidence for Modifying the Current Physical Model for Ice Accretion on Aircraft Surfaces, Cleveland, OH, United States, 1986. doi:19880003091.
[20] A. Feo, Icing Scaling with Surface Film Thickness Similarity for High LWC Conditions, in: Madrid INTA (Instituto Nac. Tec. Aeroesp. Rep., 2000. p. AE/PRO/4420/184/INTA/00, 13pp. <https://scholar.google.com/scholar?hl=en&q=Icing+scaling+with+surface+film+thickness+similarity+for+high+LWC+conditions&btnG=&as_sdt=1%2C16&as_sdtp=#0> (accessed February 16, 2016).
[21] T.G. Myers, C.P. Thompson, Modeling the flow of water on aircraft in icing conditions, AIAA J. 36 (1998) 1010–1013.
[22] X. Wang, E. Bibeau, G.F. Naterer, Experimental correlation of forced convection heat transfer from a NACA airfoil, Exp. Therm. Fluid Sci. 31 (2007) 1073–1082.
[23] X. Wang, G. Naterer, E. Bibeau, Convective heat transfer from a NACA airfoil at varying angles of attack, J. Thermophys. Heat Transf. 22 (2008) 457–463.

[24] R.V Arimilli, E.G. Keshock, M.E. Smith, Measurements of local convective heat transfer coefficients on ice accretion shapes, in: AIAA 22nd Aerosp. Sci. Meet. Reno, Nevada, 1984.
[25] D. Anderson, A. Feo, Ice-accretion scaling using water-film thickness parameters, in: 40th AIAA Aerosp. Sci. Meet. Exhib., American Institute of Aeronautics and Astronautics, Reston, Virigina, 2002. p. AIAA2002-0522. http://doi.org/10.2514/6.2002-522.
[26] M.B. Bragg, M.J. Cummings, S. Lee, C.M. Henze, Boundary-layer and heat-transfer measurements on an airfoil with simulated ice roughness, AIAA Pap. 866 (1996) 1–16.
[27] F.P. Incropera, Fundamentals of Heat and Mass Transfer, John Wiley & Sons, 2011.
[28] H. Schlichting, K. Gersten, K. Gersten, Boundary-layer Theory, Springer Science & Business Media, 2000.
[29] X. Li, J. Bai, K. Wang, Y. Shi, The application of Eulerian two-phase flow method in airfoil ice accretion, Sin-Phys. Mech. Astron. 44 (2014) 258–266.
[30] W. Dong, J. Zhu, M. Zheng, Y. Chen, Thermal analysis and testing of nonrotating cone with hot-air anti-icing system, J. Propuls Power. 31 (3) (2015) 896–903.
[31] D.M. Murphy, T. Koop, Review of the vapour pressures of ice and supercooled water for atmospheric applications, Q. J. R. Meteorol. Soc. 131 (2005) 1539–1565, https://doi.org/10.1256/qj.04.94.
[32] M. Papadakis, G.W. Zumwalt, R. Elangonan, G.A. Freund, M. Breer, L. Whitmer, An Experimental Method for Measuring Water Droplet Impingement Efficiency on Two- and Three-dimensional Bodies, Technical Report, NASA-CR-4257, NASA, United States, 1989.
[33] S.H. Davis, Theory of Solidification, Cambridge University Press, Cambridge, UK, 2001.
[34] S. Jung, M.K. Tiwari, N.V. Doan, D. Poulikakos, Mechanism of supercooled droplet freezing on surfaces, Nat. Commun. 3 (2012) 615.
[35] K. Zhang, T. Wei, H. Hu, An experimental investigation on the surface water transport process over an airfoil by using a digital image projection technique, Exp. Fluids 56 (2015) 173, https://doi.org/10.1007/s00348-015-2046-z.
[36] Y. Liu, W.-L. Chen, L.J. Bond, H. Hu, An experimental study on the characteristics of wind-driven surface water film flows by using a multi-transducer ultrasonic pulse-echo technique, Phys. Fluids 29 (2017) 12102, https://doi.org/10.1063/1.4973398.
[37] R.J. Hansman, S.R. Turnock, Investigation of surface water behavior during glaze ice accretion, J. Aircr. 26 (1989) 140–147.
[38] R.M. Waldman, H. Hu, High-SpeedImaging to Quantify Transient Ice Accretion Process over an Airfoil, J. Aircr. 53 (2015) 369–377, https://doi.org/10.2514/1.C033367.
[39] S. Özgen, M. Canıbek, Ice accretion simulation on multi-element airfoils using extended Messinger model, Heat Mass Transf. 45 (2009) 305–322, https://doi.org/10.1007/s00231-008-0430-4.
[40] D.G.K. Aboud, A.-M. Kietzig, Splashing threshold of oblique droplet impacts on surfaces of various wettability, Langmuir 31 (2015) 10100–10111, https://doi.org/10.1021/acs.langmuir.5b02447.
[41] N. Dukhan, K.J. De Witt, K.C. Masiulaniec, G.J. Van Fossen, Experimental Frossling numbers for ice-roughened NACA 0012 airfoils, J. Aircr. 40 (2003) 1161–1167, https://doi.org/10.2514/2.7205.
[42] P.E. Poinsatte, G. James, V. Fossen, K.J. Dewitt, G.J. Vanfossen, K.J. Dewitt, Convective heat transfer measurements from a NACA 0012 airfoil in flight and in the NASA Lewis Icing Research Tunnel, in: 27th AIAA Aerosp. Sci. Meet., 1989, pp. 8–11.
[43] J.E. Newton, G.J. Vanfossen, P.E. Poinsatte, K.J. Dewitt, Measurement of local convective heat transfer coefficients from a smooth and roughened NACA-0012 airfoil: Flight test data, 1988.
[44] Y. Liu, L. Li, Z. Ning, H. Hu, An experimental study on the transient ice accretion process over a rotating UAV propeller, in: 55th AIAA Aerosp. Sci. Meet. Grapevine, Texas, January 9–13, 2017, 2017.
[45] R.C. Henry, D. Guffond, Fran-atilde, O. Garnier, André, Bouveret, Heat transfer coefficient measurement on iced airfoil in small icing wind tunnel, J. Thermophys. Heat Transf. 14 (2000) 348–354.